Geosynthetics: Leading the Way to a Resilient Planet – Biondi et al (eds)

Physical and numerical study of load transfer mechanism of geotextile-reinforced sand fill over soft marine clay improved by deep cement mixed soil columns

P.C. Wu
The Hong Kong Polytechnic University, Hong Kong SAR, China

J.H. Lin
China Energy Engineering Group Guangdong Electric Power Design Institute Co. Ltd., China

W.Q. Feng
Southern University of Science and Technology, Shenzhen, China

J.H. Yin
The Hong Kong Polytechnic University, Hong Kong SAR, China

ABSTRACT: The Hong Kong International Airport has expanded its existing two-runway system to a three-runway system based on a reclamation project over a seabed of soft marine clay. In the reclamation area, a layer of load transfer platform (LTP) was designed with geosynthetic reinforcement to bridge the overlaid surcharge loadings of reclamation fills and underlaid marine clay improved by deep cement mixing method. In this study, firstly, a small-scale physical model test of geotextile-reinforced sand layer over soft marine clay improved by cement-treated soil columns was performed to investigate the load transfer mechanism among columns, soils, and geotextile under different surcharge loadings. The results from the scaled model test were then adopted to verify the parameters used in a finite element model established using PLAXIS. Furthermore, the finite element model was used to reveal the development of soil arching.

1 INTRODUCTION

The third runway reclamation project of the Hong Kong International Airport has been constructed over a seabed of soft marine clay improved by deep cement mixing (DCM) method. A layer of geosynthetic-reinforced load transfer platform (LTP) was designed in between the reclamation fills and the DCM-treated marine clay seabed (Lee 2016). The consideration of the load transfer mechanism and the design of geosynthetic reinforcements in LTP are similar to geosynthetic-reinforced column-supported (GRCS) embankments. The load transfer in a GRCS embankment is normally related to soil arching effect which develops with the settlement of subsoils or the deflection of geosynthetic reinforcements (Iglesia *et al*. 2014; King *et al*. 2017; Zhang *et al*. 2022). Various theories and models for soil arching in column-supported embankments were proposed based on empirical methods or analytical approaches, among which the semi-spherical arches model proposed by Hewlett and Randolph (1988), multi-shell arches model proposed by Zaesek (2001), and concentric arches (CA) model proposed by van Eekelen *et al*. (2013) have been adopted in British, German, and Dutch design guidelines.

In this study, a small-scale physical model test was conducted on a geotextile-reinforced sand layer over a soft subsoil improved using cement-treated soil columns to investigate the load transfer mechanism and tensile strains of the geotextile reinforcement. In addition, a numerical simulation was performed using PLAXIS software to reveal the development of the soil arching in the geotextile-reinforced sand layer at different stages.

DOI: 10.1201/9781003386889-136

2 EXPERIMENT

2.1 *Test setup*

The physical model test was conducted in a steel tank with the dimension of 1000 mm (length) × 600 mm (width) × 800 mm (depth). Six prefabricated cement-treated soil columns with a cement content of 20% (in terms of dry mass of soil) were installed in the subsoil of Hong Kong marine deposits (HKMD) overlaid by a geotextile-reinforced sand layer. The subsoil was prepared by consolidating the reconstituted HKMD with the initial water content of 100 % under a uniform load of 5.35 kPa. The columns were subsequently installed using the replacement method adopted by Ho *et al.* (2020). A sand layer (thickness of 350 mm) over the HKMD was filled in seven times with a 50 mm thick sublayer formed each time after compaction. The total weight and volume of sand were controlled to ensure a relative density of 80%. A piece of woven geotextile (secant tensile modulus of 680 and 150 kN/m in longitudinal and transversal directions) was installed 50 mm above the subsoil, as shown in Figure 1. A rigid porous plate was placed on the top of the sand layer to serve as a platform for setting the LVDTs (manufactured by SHOWA) and as a loading plate. Earth pressure cells (EPCs) and porewater pressure transducers (PPTs), manufactured by DMKY, were used to measure the vertical stress and excess porewater pressure at different locations. Fiber Bragg grating (FBG) sensors (manufactured by T&S) were adopted to measure the tensile strain of the geotextile reinforcement. NI PXIE 4331 datalogger was used to record electronic signals from all conventional transducers. FBG-based transducers were connected to Micron Optics SM130 interrogator.

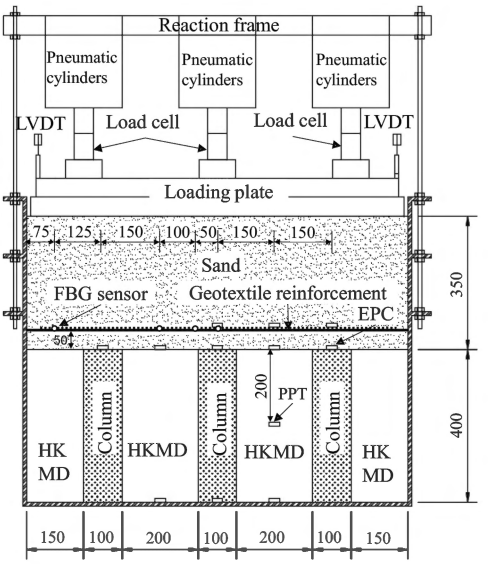

Figure 1. Schematic diagram of the physical model test (unit in mm).

2.2 *Test results*

The surcharge loading was applied by pneumatic cylinders following a loading sequence of 10, 20, 40, and 80 kPa. Each loading stage lasted until there was no further change in excess porewater pressure. Figure 2a shows the average surface settlement measured by LVDTs and the actual loading applied to the top of the sand layer measured by load cells. The responses of excess porewater pressure measured by PPTs at the middle and bottom levels of the subsoil are presented in Figure 2b. Rapid dissipation of excess porewater pressure at both

locations can be observed at the very beginning of each loading stage. The accelerated consolidation was mainly because of the mechanical contribution of the columns on loading transfer (Wijerathna *et al*. 2017; Wu *et al*. 2020).

Different terminologies and definitions were proposed to assess the soil arching effect and interpret load transfer mechanisms. In this study, pile (or column) efficacy, proposed by Hewlett and Randolph (1988), is adopted:

$$E = \frac{A + B}{(\gamma H + p)s^2} \tag{1}$$

where A and B represent load parts A and B defined by van Eekelen *et al*. (2013); p is the surcharge loading; s is the center-to-center spacing of columns; γ and H are the unit weight and height of the sand layer. Load parts A and B are calculated as follows:

$$A = \sigma_c^a A_c \tag{2}$$

$$B = \left(\sigma_c^b - \sigma_c^a\right) A_c \tag{3}$$

where σ_c^a and σ_c^b are the average vertical stresses measured by EPCs above and beneath the geotextile reinforcement in column zones; A_c is the area of column zones. Figure 2c presents the values of efficacy with different surcharge loadings. It is found that the efficacy decreases during the process of increasing the surcharge loading. This is because of the partially undrained condition of the subsoil delays the loading transfer. With the consolidation of the subsoil under the given surcharge loading, differential settlements between columns and the surrounding soils increase inducing an increase in the deflection of the geotextile reinforcement, and thus leading to an increase in efficacy. The efficacy of columns after the consolidation slightly increases with the increase of the surcharge loading. This finding agrees with the simulation results from van der Peet and van Eekelen (2014).

Figure 2d presents the maximum tensile strains in both longitudinal (x) and transversal (y) directions of the geotextile reinforcement. The maximum tensile strains under different surcharge loadings can be also calculated according to Dutch design guidelines (van Eekelen & Brugman 2016) and German design guidelines (EBGEO 2010). It is found that the Dutch method gives better predictions in terms of the maximum tensile strains of geotextile reinforcement when the surcharge loading was less than 40 kPa, while German EBGEO method provides closer results to the measured strains under 80 kPa.

3 NUMERICAL SIMULATIONS

3.1 *FE models*

A 3D finite element (FE) model of four quarter columns and HKMD subsoil is built using PLAXIS 3D, as shown in Figure 3. HKMD subsoil is simulated by Soft Soil Creep (SSC) model, cement-treated soil columns are simulated by Mohr-Coulomb (MC) model, the sand layer is simulated by Hardening Soil (HS) model, the geotextile reinforcement is simulated by geogrid elements with elastic properties. Table 1 lists the input parameters for the simulation. Standard boundary conditions with the bottom boundary fixed in all directions, side boundaries normally fixed, and top boundary free are applied to the FE model. Horizontal interfaces are assigned on both sides of the geotextile reinforcement facing to overlaid and underlaid sand layers. A reduction factor of 0.8 is selected to consider the interfacial friction angle between the sand and geotextile reinforcement (Yapage & Liyanapathirana 2018). Vertical interfaces are assigned between DCM columns and HKMD. Similar to the FE models of van der Peet *et al*. (2014), the vertical interfaces are extended 0.1 m into the overlying sand layer. The properties of the extended interface are identical to the

surrounding sand. The FE model is meshed into 55446 10-noded soil (tetrahedrons) elements. In order to consider large deformation and the membrane effect of the geotextile reinforcement, the function of updated generated mesh should be utilized.

3.2 *Simulation results*

Selected observation points for checking the simulation results are marked in Figure 3. Figure 2a presents the simulated settlement at observation point *a*, representing the surface settlement. Good agreement can be seen from the simulated settlement and measured settlement. The simulated excess porewater pressures at observation points *d* and *e* represent the excess porewater pressures measured by PPTs at the middle and bottom levels, as shown in Figure 2b. Similar to Section 2.2, efficacy can be calculated based on the simulated vertical stresses. It can be seen from Figure 2c that the simulation results agree well with the test results.

The simulated tensile strains of the geotextile reinforcement are calculated as:

$$\varepsilon_{x,y} = \frac{T_{x,y}}{J_{x,y}} \tag{4}$$

where $\varepsilon_{x,y}$, $T_{x,y}$, and $J_{x,y}$ are the tensile strain, force, and stiffness in x and y directions, respectively. Figure 2d shows the comparison between the simulated and measured maximum tensile strains of the geotextile reinforcement under different surcharge loadings. It is found that the FE simulation underestimated the maximum tensile strain. This difference between the simulation and test results might be mainly attributed to that the geotextile reinforcement was treated as a linear elastic material in the FE model.

Table 1. Parameters for different materials.

Material	Model	Parameter
HKMD*	SSC	γ_{sat} = 16.5 kN/m^3; λ^* = 0.107; κ^* = 0.027; μ^* = 0.002037; ν = 0.15; c' = 0.5 kPa; φ' = 24°; $k_{x,y}$ = 7.0×10^{-4} m/day; k_z = 3.5×10^{-4} m/day; POP = 5 kPa
Columns	MC	γ_{sat} = 16.5 kN/m^3; E'_{50} = 40 MPa; ν = 0.25; c' = 80 kPa, φ' = 42°;
Sand**	HS	γ_{sat} = 17.5 kN/m^3; E'_{50} = 30 MPa; E'_{oed} = 20 MPa; E'_{ur} = 90 MPa; m = 0.5; ν = 0.2; c' = 0.1 kPa, φ' = 34.6°; ψ' = 4.6°; POP = 10 kPa; p_{ref} = 100 kPa
Geotextile	Elastic	$J_{x,y}$ = 680,150 kN/m

*The parameters used in SSC model were determined from oedometer and triaxial tests on reconstituted HKMD.

**The parameters used in HS model were determined from CD triaxial tests on sand.

The shape and size of soil arches are usually assumed in different arching models and design guidelines of GRCS embankments (Lee *et al*. 2021). The calculation of load part *A* highly depends on the shape and size of soil arches. van der Peet *et al*. (2014) considered that the principal stress is parallel to the arches and verified CA model by presenting the directions of principal stress. To investigate soil arching in the physical model test of this study, principal stress directions between two adjacent columns and those between two diagonal columns at different stages are presented in Figure 4. The case with a surcharge loading of 40 kPa is taken as an example to show the difference between the simulation results and CA model in terms of the shape of arches. The arches determined from this study are denoted by dotted curves while the outmost arches determined according to CA model are represented

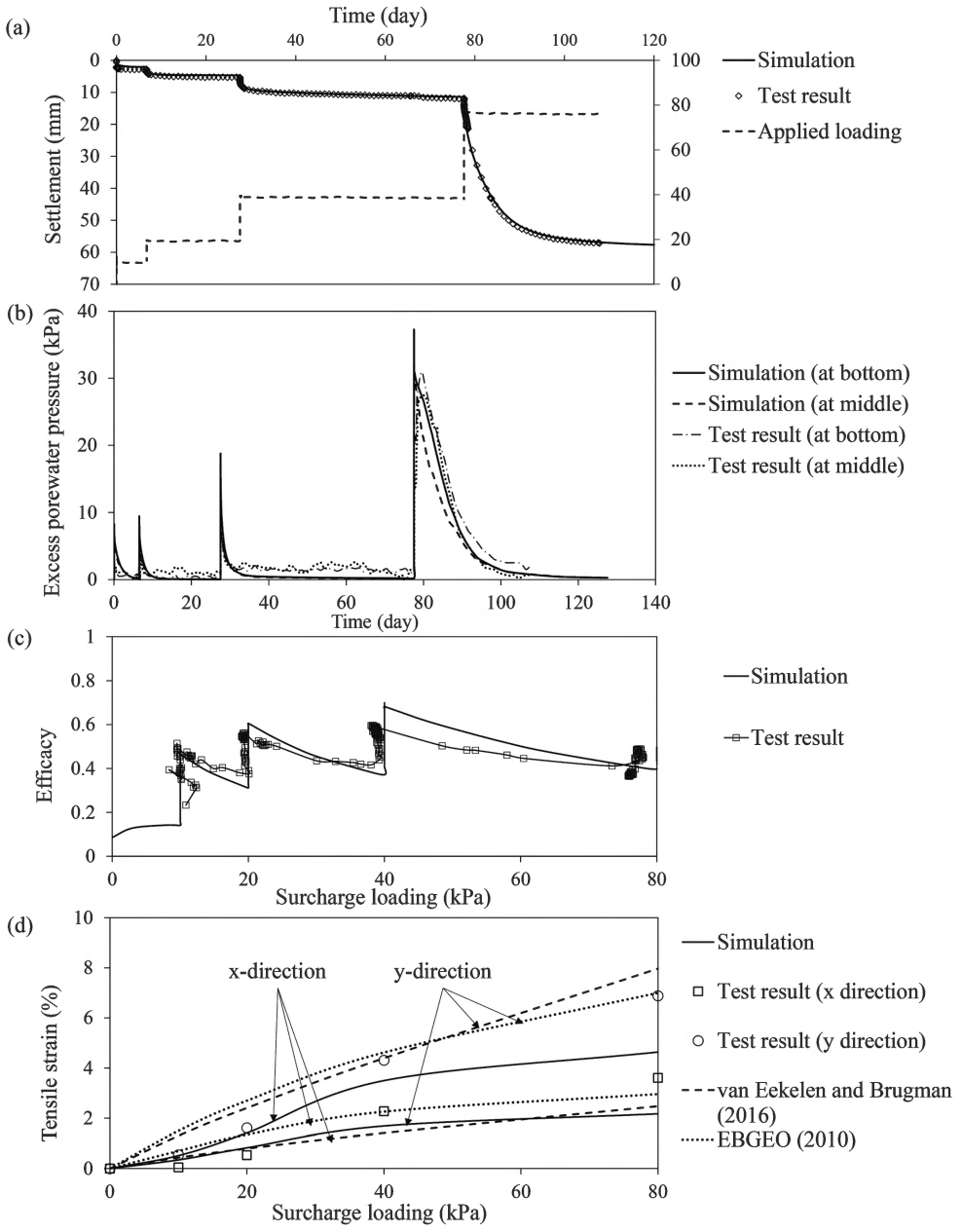

Figure 2. Experimental and numerical results of (a) surface settlement, (b) excess porewater pressures, (c) column efficacy, (d) tensile strains.

by dashed curves. It can be seen from Figures 4a and b that the shape of arches between adjacent columns and between diagonal columns are quite different from those determined by CA model at the loading stage. Triangular arches similar to those shown in Figure 4a were also found by Rui *et al.* (2016) and van Der Peet and van Eekelen (2014) using 2D trapdoor tests and numerical simulation, respectively. After the consolidation of the HKMD

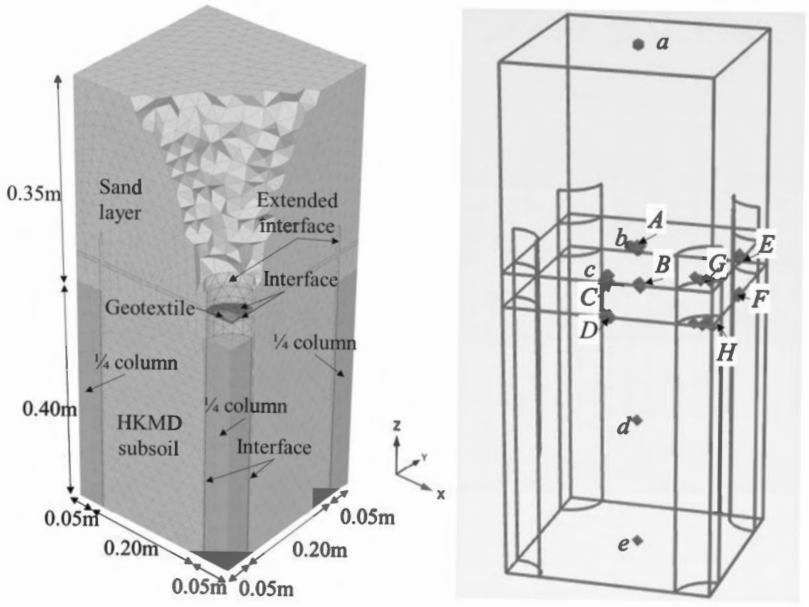

Figure 3. Illustration of the FE model and locations of observation points.

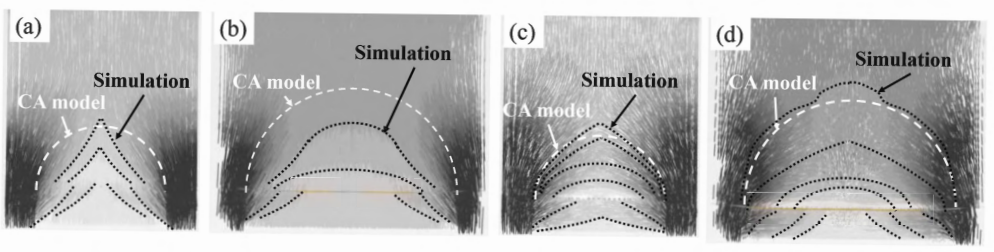

Figure 4. The shape of soil arches: (a) between two adjacent columns at loading stage, (b) between two diagonal columns at loading stage, (c) between two adjacent columns after consolidation, and (d) between two diagonal columns after consolidation.

subsoils, the inner triangular arches between two adjacent columns tended to become concentric semi-circular arches, which agrees with the assumption of CA model about the shape of arches. More clear concentric arches can be also observed between two diagonal columns. Although the outermost arches determined from the simulation results are triangular between two adjacent columns and bell-shaped between two diagonal columns, their sizes are similar to those determined by CA model.

4 CONCLUSIONS

A physical model test on geotextile-reinforced sand fill over soft marine clay improved by DCM columns has been successfully conducted with the measurement of earth pressures and the tensile strains of the geotextile reinforcement. The tensile strains calculated according to Dutch design guidelines agree with the measured data. Soil arching developed during loading stages and after the consolidation of the subsoil was revealed using the verified finite

element method and compared with CA model. Unlike the ideal concentric semi-spherical arches assumed in CA model, the shape of the arches observed in the simulation is more complicated.

ACKNOWLEDGEMENTS

The work in this paper is supported by a Research Impact Fund (RIF) project (R5037-18) and a General Research Fund (GRF) project (PolyU 15226722) from Research Grants Council (RGC) of Hong Kong SAR Government.

REFERENCES

EBGEO 2010. *Empfehlungen für den Entwurf und die Berechnung von Erdkörpern mit Bewehrungen aus Geokunststoffen e EBGEO*, vol. 2 German Geotechnical Society, Auflage978-3-433-02950-3 (in German). Also available in English: Recommendations for Design and Analysis of Earth Structures using Geosynthetic Reinforcements e EBGEO, 2011. ISBN: 978-3-433-02983-1 and digital in English ISBN: 978-3-433-60093-1.

Hewlett, W. J. 1988. Analysis of Piled Embankment. *Ground Engrg.* 21(3): 12–18.

Ho, T. O., Tsang, D. C., Chen, W. B., & Yin, J.H. 2020. Evaluating the Environmental Impact of Contaminated Sediment Column Stabilized by Deep Cement Mixing. *Chemosphere* 261: 127755.

Iglesia, G.R., Einstein, H.H., & Whitman, R.V. 2014. Investigation of Soil Arching with Centrifuge Tests. *Journal of Geotechnical and Geoenvironmental Engineering* 140(2): 04013005.

King, D.J., Bouazza, A., Gniel, J.R., Rowe, R.K., & Bui, H.H. 2017. Load-transfer Platform Behaviour in Embankments Supported on Semi-rigid Columns: Implications of the Ground Reaction Curve. *Canadian Geotechnical Journal* 54(8): 1158–1175.

Lee D. 2016. Expansion of Hong Kong International Airport into a Three-Runway System, Airport Reclamations – then and now. HKIE YMC Seminar. http://ymc.hkie.org.hk/DocDown.aspx?imgDoc=151_160120+3RS+Reclamation+(20+Jan+2016).pdf

Lee, T., Van Eekelen, S. J., & Jung, Y. H. 2021. Numerical Verification of the Concentric Arches Model for Geosynthetic-reinforced Pile-supported Embankments: Applicability and Limitations. *Canadian Geotechnical Journal* 58(3): 441–454.

Rui, R., Van Tol, A. F., Xia, Y. Y., Van Eekelen, S. J. M., & Hu, G. 2016. Investigation of Soil-arching Development in Dense Sand by 2D Model Tests. *Geotechnical Testing Journal* 39(3): 415–430.

van der Peet, T. C., & Van Eekelen, S. J. M. 2014. 3D Numerical Analysis of Basal Reinforced Piled Embankments. *In Tenth International Conference on Geosynthetics* (pp. 21–25).

van der Peet, T. C., Van Duijnen, P. G., Van Eekelen, S. J. M., & Brinkgreve, R. B. J. 2014. Validating a New Design Method for Piled Embankments with Plaxis 2D and 3D. *in Plaxis bulletin*.

van Eekelen, S.J.M., Bezuijen, A., & Van Tol, A.F. 2013. An Analytical Model for Arching in Piled Embankments. *Geotextiles and Geomembranes* 39: 78–102.

van Eekelen, S.J., & Brugman, M.H. 2016. *Design Guideline Basal Reinforced Piled Embankments*. CRC Press.

Wijerathna, M., Liyanapathirana, D. S., & Jian Leo, C. 2017. Analytical Solution for the Consolidation Behavior of Deep Cement Mixed Column–improved Ground. *International Journal of Geomechanics* 17(9): 04017065.

Wu, P. C., Feng, W. Q., & Yin, J. H. 2020. Numerical Study of Creep Effects on Settlements and Load Transfer Mechanisms of Soft Soil Improved by Deep Cement Mixed Soil Columns Under Embankment Load. *Geotextiles and Geomembranes* 48(3): 331–348.

Yapage, N., & Liyanapathirana, S. 2018. Behaviour of Geosynthetic Reinforced Column Supported Embankments. *Journal of Engineering, Design and Technology* 16(1): 44–62.

Zaeske, D. 2001. *Zur Wirkungsweise von Unbewehrten und Bewehrten Mineralischen Tragschichten Über Pfahlartigen Gründungselementen*. Fachgebiet u. Versuchsanst. Geotechnik, Univ. Gh Kassel.

Zhang, C., Su, L., & Jiang, G. 2022. Full-scale Model Tests of Load Transfer in Geogrid-reinforced and Floating Pile-supported Embankments. *Geotextiles and Geomembranes* 50(5):896–909.